


Resonating dimer–monomer liquid state in a magnetization plateau of a spin- $\frac{1}{2}$ kagome-strip Heisenberg chain

Katsuhiko Morita^{1,2}, Shigetoshi Sota³ & Takami Tohyama¹

Highly frustrated spin systems such as the kagome lattice are a treasure trove of new quantum states with large entanglements. Herein, we study the spin- $\frac{1}{2}$ Heisenberg model on a kagome-strip chain, which is a one-dimensional kagome lattice, using the density matrix renormalization group method. Calculating the central charge and entanglement spectrum for the kagome-strip chain, we find a gapless spin liquid state with doubly degenerate entanglement spectra in a $1/5$ magnetization plateau. We also obtain a gapless low-lying continuum in the dynamic spin structure calculated using the dynamical density matrix renormalization group method. We then propose a resonating dimer–monomer liquid state that meets these features.

¹Department of Applied Physics, Tokyo University of Science, Tokyo, Japan. ²Graduate School of Arts and Sciences, The University of Tokyo, Tokyo, Japan. ³RIKEN Center for Computational Science (R-CCS), Kobe, Hyogo, Japan. ✉email: katsuhiko.morita@rs.tus.ac.jp

Quantum entanglement is an extremely important concept in research, such as quantum information and quantum magnetism¹. Low-dimensional quantum spin systems are attracting attention because they are expected to have a strong entanglement. A quantum entanglement analysis for quantum spin models has recently attracted attention because it can characterize various phases^{2–10}, even in states without a break in the translational symmetry or long-range dipole orders, such as the Haldane state in integer spin chains¹¹ and the Tomonaga–Luttinger liquid (TLL) state in half-integer spin chains. According to conformal field theory, the central charge c characterizing the excitation properties can be obtained by calculating the entanglement entropy^{2–6}. In a TLL state, there is a gapless excitation with a non-zero integer value of c , whereas in a Haldane state, there is a gapped excitation with $c = 0$. Moreover, the Haldane state can be characterized by the degeneracy of the entanglement spectrum^{7–10}. For example, the spin-1 chain exhibits a doubly degenerate entanglement spectrum⁷.

In two-dimensional frustrated quantum spin systems, quantum spin liquid states, such as the resonating valence bond (RVB) introduced by Anderson, are expected to emerge^{12,13}. The RVB state is a resonant state of singlet dimers covering the whole lattice. It is believed that one of the possible models for exhibiting RVB states is the spin- $\frac{1}{2}$ antiferromagnetic Heisenberg model on the kagome lattice¹⁴. However, the ground state has been predicted to be a Z_2 RVB spin liquid with topological order^{14–17}, U(1) spin liquid^{18–21}, and valence bond crystal (VBC)^{22–26}, although the exact ground state is unknown owing to the difficulty in solving two-dimensional frustrated systems. In the presence of a magnetic field, magnetization plateaus were predicted at $M/M_{\text{sat}} = 0, 1/9, 1/3, 5/9, \text{ and } 7/9$, where M is the magnetization and M_{sat} is the saturation magnetization^{16,27–29}. These magnetization plateaus are realized by the effect of the strong geometric frustration peculiar to the kagome lattice.

Kagome strip chains (KSCs), which are one-dimensional kagome lattices, have been recently studied, because the presence of exotic quantum states is expected in the kagome lattice^{30–37}. In the KSC, as shown in Fig. 1, it was found that the magnetization plateaus emerge at $M/M_{\text{sat}} = 0, 1/5, 3/10, 1/3, 2/5, 7/15, 3/5, \text{ and } 4/5$ ³⁵. Among them, four types of plateaus were found at $M/M_{\text{sat}} = 1/5$. The number of different types in each plateau was the largest at $M/M_{\text{sat}} = 1/5$. Therefore, we can expect the presence of quantum phases generated by a strong geometrical frustration in this $1/5$ plateau. Furthermore, when the model compound for the KSC is synthesized in the near future, the $1/5$ plateau can be easily accessed with a small magnetic field.

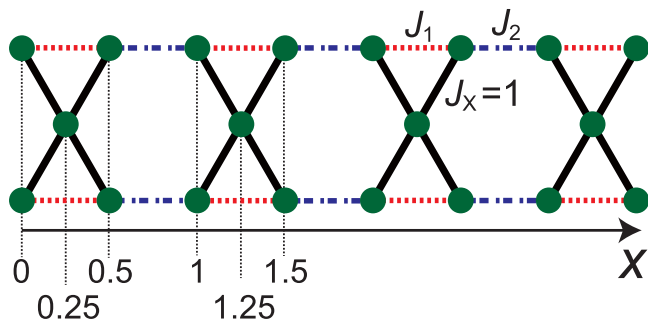


Fig. 1 Structure of a kagome-strip chain. The black solid, red dashed, and blue broken lines denote the exchange interactions J_X , J_1 , and J_2 , respectively. The green circles denote the sites with spin. The numbers below the vertical dotted lines represent the distance of the sites along the x -axis from the left edge. We set $J_X = 1$.

In this study, we investigate the $1/5$ plateaus of the KSC using the density matrix renormalization group (DMRG) method. We developed a magnetic phase diagram of the $1/5$ plateau and, to the best of our knowledge, found two new plateau phases that have yet to be identified in the previous studies³⁵. As our main result, although one of the two phases exhibits a gapless spin-liquid behavior with $c = 1$, the entanglement spectrum of the phase is doubly degenerate. This means that this plateau phase has the properties of both a half-integer spin chain and a spin-1 chain. This feature is known to be realized in the gapless symmetry-protected topological (SPT) phase, which has been studied in recent years^{38,39}. Furthermore, we calculate the dynamical spin structure factor (DSSF) in this phase using the dynamic DMRG (DDMRG)⁴⁰ (see Methods section). The DSSF of the S^z (magnetic field) direction exhibits gapless and dispersion-less low-energy excitations. To describe these properties during the phase, we propose a resonating dimer–monomer liquid (RDML) state, which is a mixed state of singlet dimers and up-spin monomers.

Results

Model. The unit cell of the KSC consists of one site located in the center and four sites located in the four corners. The Hamiltonian for the spin- $\frac{1}{2}$ KSC in a magnetic field is defined as

$$H = \sum_{\langle i,j \rangle} J_{ij} \mathbf{S}_i \cdot \mathbf{S}_j - h \sum_i S_i^z, \quad (1)$$

where \mathbf{S}_i is the spin- $\frac{1}{2}$ operator, S_i^z is the z component of \mathbf{S}_i , $\langle i, j \rangle$ runs over the nearest-neighbor spin pairs. The first and second terms in Eq. (1) represent the Heisenberg interaction and Zeeman interaction with the magnetic field h along the z direction, respectively. J_{ij} in the first term corresponds to one of J_X , J_1 , or J_2 in Fig. 1. J_X in Fig. 1 represents the antiferromagnetic exchange interaction between the central site and one of the other sites in the unit cell. J_1 is the exchange interaction between the nearest-neighbor sites along the upper and lower edges in the unit cell, while J_2 is the nearest-neighbor interaction along the upper and lower edges connecting neighboring unit cells. In the following, we set $J_X = 1$ as the energy unit.

Phase diagram of the kagome strip chain. We first determined the phase diagram of the KSC at $M/M_{\text{sat}} = 1/5$ using the DMRG method. We obtained six $1/5$ plateau phases using $N = 120$ – 1000 clusters under the open boundary condition (OBC), as shown in Fig. 2, where N denotes the number of sites. We determined the phase boundaries for each magnetization plateau from the magnetization curve and their magnetic structures, as shown in Fig. 3.

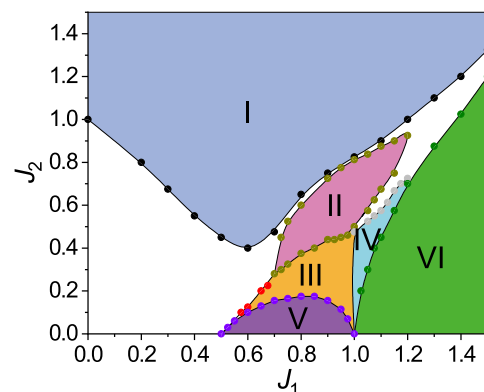


Fig. 2 Phase diagram of the kagome strip chain at $M/M_{\text{sat}} = 1/5$. M is the magnetization and M_{sat} is the saturation magnetization. Here, J_1 and J_2 are the exchange interactions shown in Fig. 1. The colored regions denote the $1/5$ plateau phases, which are distinguished by Roman numerals and colors.

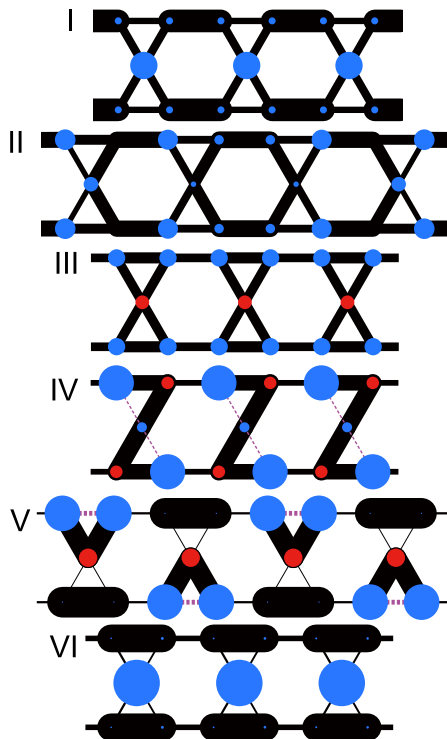


Fig. 3 Magnetic structures of each phase. The nearest-neighbor spin-spin correlation $\langle \mathbf{S}_i \cdot \mathbf{S}_j \rangle - \langle S_i^z \rangle \langle S_j^z \rangle$ and the local magnetization $\langle S_i^z \rangle$ around the center of the chain with $N = 200$ under the open boundary condition for the six phases, where \mathbf{S}_i is the spin- $\frac{1}{2}$ operator, S_i^z is the z component of \mathbf{S}_i , and N is the number of sites. Black solid (purple dashed) lines connecting two nearest-neighbor sites denote negative (positive) values of the spin-spin correlation, and their thickness represents the magnitude of the correlation. The blue (red) circles on each site denote the positive (negative) value of $\langle S_i^z \rangle$, and their diameter represents its magnitude. Roman numerals denote the 1/5 plateau phases and correspond to those in Fig. 2. In VI, the value of $\langle S_i^z \rangle$ at the center is 0.4193, and that of $\langle \mathbf{S}_i \cdot \mathbf{S}_j \rangle - \langle S_i^z \rangle \langle S_j^z \rangle$ of the thickest line is -0.6513 .

The regions of phases I–VI are denoted by different colors. The white region had no magnetization plateau. Phases II and III were found in the present study, whereas the other phases had already been found in a previous study³⁵.

Figure 3 shows the nearest-neighbor spin-spin correlation $\langle \mathbf{S}_i \cdot \mathbf{S}_j \rangle - \langle S_i^z \rangle \langle S_j^z \rangle$ and local magnetization $\langle S_i^z \rangle$ for the six phases. The lines connecting two nearest-neighbor sites denote the sign and magnitude of the spin-spin correlation by color and thickness, respectively. The circle in each site represents $\langle S_i^z \rangle$. The stability of phases I, IV, V, and VI can be explained by the energy gain owing to a local strong spin correlation, as evidenced by the thick lines in Fig. 3. By contrast, phases II and III do not have such a distinguished thick line. In phase II, the periodic magnetic structure of the spin-spin correlation and local magnetization are not observed, whereas the mirror and inversion symmetries at the center of the chain, which should exist under the OBC, are unbroken (see Supplementary Note 1). In phase III, the spin-spin correlation and local magnetization have a periodic structure, and there is no symmetry breaking.

Magnetization process and magnetization plateau. Figure 4a, b show magnetization curves at $J_1 = 1.0$ and $J_2 = 0.7$ (phase II), and $J_1 = 0.9$ and $J_2 = 0.3$ (phase III), respectively. The 1/5 plateaus are clearly visible under both conditions. These magnetization curves show little variation with size N and the boundary conditions.

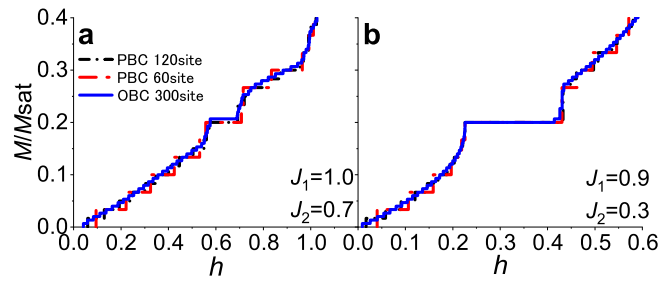


Fig. 4 Magnetization curves in phases II and III as a function of the magnetic field. The black, red, and blue solid lines show the results of the periodic boundary condition for $N = 60$, periodic boundary condition for $N = 120$, and open boundary condition for $N = 300$, respectively, at zero temperature, where N is the number of sites. In addition, M is the magnetization, M_{sat} is the saturation magnetization, and h is the magnitude of the magnetic field. **a** $J_1 = 1.0$ and $J_2 = 0.7$ (phase II). **b** $J_1 = 0.9$ and $J_2 = 0.3$ (phase III). J_1 and J_2 are the exchange interactions shown in Fig. 1.

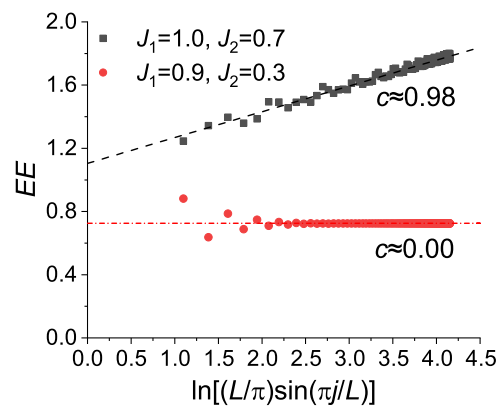


Fig. 5 Entanglement entropy of the kagome strip chain. The cluster used in the calculations is the open boundary condition for $L = 200 (N = 5 \times 200)$, where L is the number of five-site units in the kagome strip chain. The results of the calculation of the entanglement entropy with respect to $\ln[L/\pi \sin(\pi j/L)]$ at $J_1 = 1.0$ and $J_2 = 0.7$ (Phase II), and $J_1 = 0.9$ and $J_2 = 0.3$ (Phase III), are represented by black squares and red circles, respectively, where j denotes the position of the 5-site unit. Here, J_1 and J_2 are the exchange interactions shown in Fig. 1. The value of the central charge c was obtained by fitting the entanglement entropy data using straight lines. The fitting lines are shown as dashed lines.

However, in Fig. 4a (phase II), a plateau deviating from 1/5 in only one step, that is, $M/M_{\text{sat}} = 1/5 + 2/N$, appears under the OBC. We confirmed that this deviation appears in the other sets of J_1 and J_2 in phase II, implying the presence of edge excitations that appear in the Haldane chain. For example, in the spin-1 Haldane chain under the OBC, the magnetization plateau does not appear at $M = 0$ but at $M = 1$. This is because two spins at both ends of the chain cannot form a valence bond, and thus both spins have almost spin-1/2 degrees of freedom, forming an $M = 1$ state under a magnetic field⁴¹. We also confirm the excitation owing to the edge spins in phase II (see Supplementary Note 1). In the following, we regard the 1/5 plateau in phase II under the OBC as the state with $M/M_{\text{sat}} = 1/5 + 2/N$. Phases I, IV, V, and VI were examined in a previous study^{??}. Therefore, we investigate phases II and III in the following.

Evidence of spin liquid in phase II form the central charge. Figure 5 shows the entanglement entropy for $L = 200 (N = 5 \times L)$ under the OBC as a function of $\ln[L/\pi \sin(\pi j/L)]$ with a variable j denoting the position of the 5-site unit. This plot comes from the

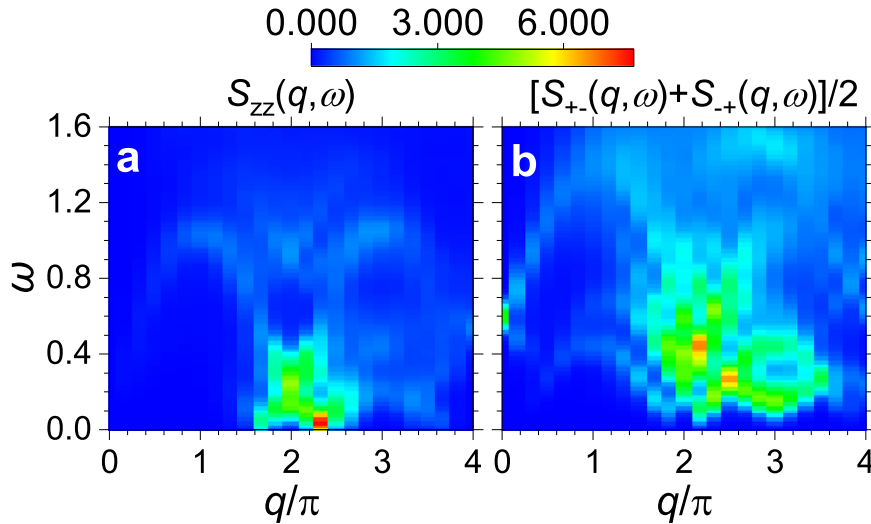


Fig. 6 Dynamical spin structure factor of phase II. **a** $S_{zz}(q, \omega)$ and **b** $[S_{+-}(q, \omega) + S_{-+}(q, \omega)]/2$, obtained from the dynamic density matrix renormalization group for the kagome strip chain under the periodic boundary condition for $L = 12$ ($N = 5 \times 12$) at $J_1 = 1.0$ and $J_2 = 0.7$, where L is the number of the 5-site units, and J_1 and J_2 are the exchange interactions shown in Fig. 1. In addition, $S_{zz}(q, \omega)$ corresponds to the S^z component of the dynamical spin structure factor, and $[S_{+-}(q, \omega) + S_{-+}(q, \omega)]/2$ correspond to the S^x and S^y components.

following relation between the central charge c and the position-dependent entanglement entropy, $EE(j)$:

$$EE(j) = \frac{c}{b_c} \ln \left[\frac{L}{\pi} \sin \left(\frac{\pi j}{L} \right) \right] + a_c, \quad (2)$$

where a_c is a nonuniversal constant, and $b_c = 6$ (3) for the OBC (PBC)^{3–6}. The value of c becomes finite when the spin-spin correlation exhibits a power-law decay, and gives $c = 1$ in the TLL. By contrast, when the spin-spin correlation decays exponentially, e.g., in the Haldane phase, $c = 0$. The value of c in Fig. 5 was obtained by fitting the entanglement entropy data using straight lines. Because c for phase II is nearly unity, as in the TLL, phase II is expected to be a gapless spin liquid. Because plateau phases should have an energy gap, there should be a gapless excitation only in the subspace where the total S^z does not change. This feature has also been observed in the $1/3$ magnetization plateau in frustrated three-leg spin tubes^{42–44}. We also confirm that the spin-spin correlations of the S^z and S^x components exhibit a power decay corresponding to the gapless excitation and exponential decay corresponding to the energy gap, respectively (see Supplementary Note 2).

In phase III, c is nearly zero. This indicates that there is an energy gap in this phase. Moreover, we confirm that the ground state has no degeneracy, and there is no symmetry breaking, as shown in Fig. 3. We note that when the ground state has no degeneracy and no symmetry breaking, the Oshikawa–Yamanaka–Affleck (OYA) criterion⁴⁵ which is given by $pS(1 - M/M_{\text{sat}}) = n$ must be satisfied, where p is the ground-state period, S is the spin magnitude, and n is an integer. In phase III, the OYA criterion is satisfied because $p = 5$, $S = 1/2$, $M/M_{\text{sat}} = 1/5$ gives integer $n = 2$.

Continuous excitation in dynamical spin structure factor. To investigate phase II in more detail, we calculate the DSSF, $S_{\alpha\beta}(q, \omega)$, which is defined by

$$S_{\alpha\beta}(q, \omega) = -\frac{1}{\pi} \text{Im} \langle 0 | \tilde{S}_{-q}^{\beta} \frac{1}{\omega - H + E_0 + i\eta} \tilde{S}_q^{\alpha} | 0 \rangle, \quad (3)$$

where q denotes the momentum of the lattice geometry shown in Fig. 1, $|0\rangle$ is the ground state with energy E_0 , and η is the broadening factor. In addition, $\tilde{S}_q^{\alpha(\beta)} = S_q^{\alpha(\beta)} - \langle 0 | S_q^{\alpha(\beta)} | 0 \rangle$, where

$$S_q^{\alpha(\beta)} = N^{-1/2} \sum_i e^{iqx_i} S_i^{\alpha(\beta)}, \quad x_i \text{ is the position of the spin } i, \text{ and } \alpha(\beta) = +, -, z.$$

Figure 6 shows $S_{zz}(q, \omega)$ corresponding to the S^z component and $[S_{+-}(q, \omega) + S_{-+}(q, \omega)]/2$ corresponding to the S^x and S^y components for $L = 12$ ($N = 5 \times 12$) with $\eta = 0.05$ under the PBC. Because the position x_i is defined in Fig. 1, the range of $0 \leq q/\pi \leq 4$ corresponds to half of the extended Brillouin zone. As shown in Fig. 6a, a gapless excitation in the S^z component emerges at approximately $q/\pi = 2$. This excitation is consistent with the expected result from the fact that $c = 1$. We confirm that the value of q showing the lowest-energy excitation is size-dependent. As the size increases, the q value tends to move toward 2π (see Supplementary Note 3). Thus, we expect that in the thermodynamic limit, a gapless excitation emerges at $q/\pi = 2$. In addition, low-energy excitations at $\omega \lesssim 0.2$ show a less dispersive feature. This feature will be discussed later.

As shown in Fig. 6b, $[S_{+-}(q, \omega) + S_{-+}(q, \omega)]/2$, corresponding to the excitations of the S^+ and S^- components, has a gap. Here, the external magnetic field h is set to 0.63, which is the value at the center of the $1/5$ magnetization plateau. The minimum excitation gap is found to exist at approximately $q/\pi = 2$ and $q/\pi = 3$. Continuous excitations exist up to the high-energy region at more than $\omega = 1.5$ at $q/\pi = 2$.

Entanglement spectrum with double degeneracy in phase II. Finally, we calculated the entanglement spectrum to investigate each phase in more detail. The ground state can be Schmidt decomposed as follows:

$$|0\rangle = \sum_{\alpha} \lambda_{\alpha} |\Phi_{\alpha}^L\rangle |\Phi_{\alpha}^R\rangle, \quad (4)$$

where $|\Phi_{\alpha}^L\rangle$ and $|\Phi_{\alpha}^R\rangle$ are orthonormal basis vectors of the left and right part of the chain, respectively⁷. Here, λ_{α}^2 are the eigenvalues of the reduced density matrix. The entanglement spectrum is defined as $-2\ln(\lambda_{\alpha})$. Figure 7 shows the results of the entanglement spectrum as a function of J_2 at $J_1 = 0.9$. Phases I, III, and V are trivial phases owing to the mixture of singly and doubly degenerate states of the entanglement spectrum⁷. By contrast, in phase II, all the entanglement spectra are doubly degenerate. Furthermore, in phase II, edge excitation occurs, as discussed in Discussion section. The doubly degenerated entanglement

spectrum and edge excitation are identical to the features of the spin-1 Haldane chain. Therefore, we speculate that phase II is a nontrivial topological phase⁷. However, we have not yet been able to identify the symmetry protecting the degeneracy in phase II, which remains a future study. We also confirm that the double degeneracy is independent of L , J_1 , and J_2 . Degeneracy is obtained even for $L = 2$ (the shortest chain).

Discussion

To the best of our knowledge, phases II and III are newly identified magnetization plateau phases in the present study. Phase III was concluded to be a trivial phase based on (i) $c = 0$, (ii) no degeneracy in the ground state, and (iii) a trivial distribution of the entanglement spectrum. By contrast, phase II is a phase that has the characteristics of both a gapless spin liquid and spin-1 Haldane state because of $c = 1$ and the double degeneracy of the entanglement spectrum. These characteristics are the same as those of the gapless SPT phase^{38,39}.

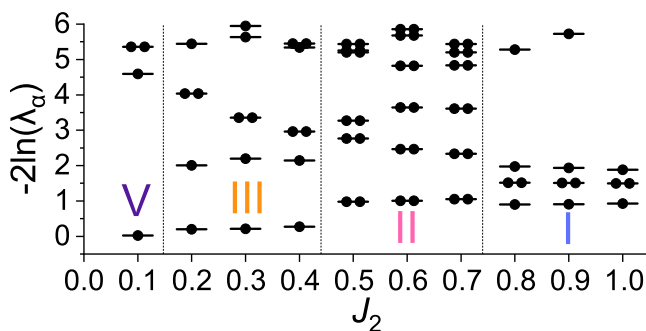


Fig. 7 Entanglement spectrum of the kagome strip chain with respect to J_2 at $J_1 = 0.9$. Here, J_1 and J_2 are the exchange interactions shown in Fig. 1. The cluster used in the calculations is the open boundary condition for $L = 80$ ($N = 5 \times 80$), where L is the number of five-site units in the kagome strip chain. In addition, λ_α^2 are the eigenvalues of the reduced density matrix, and α is an index of the eigenvalues. The Roman numerals correspond to the phases shown in Fig. 2. The vertical dotted lines represent the phase boundaries determined by the entanglement spectrum and the magnetic structures. The horizontal bars indicate the values of λ_α , and the filled circles indicate the degeneracy of λ_α .

Why does phase II have these characteristics? We anticipate that a mixed state of singlet dimers and up-spin monomers, which reveals a liquid behavior similar to the RVB, is the ground state of phase II. We refer to this state as RDML. The RDML state in the KSC under the OBC is introduced as $|\psi\rangle_{\text{RDML}} = \sum_i a_i |\phi_i\rangle_{\text{DM}}$, where a_i is a constant and $|\phi_i\rangle_{\text{DM}}$ is one of the dimer–monomer states, which has only one monomer in all 5-site units except at both ends, and there is no nearest-neighboring monomer, as shown in Fig. 8. In other words, all states of $\{|\phi_i\rangle_{\text{DM}}\}$ have one dimer (not two dimers) in all 5-site units. In addition, the four spins at both ends are up-spin monomers, reflecting the results of the numerical calculation (see Supplementary Note 1). The monomers at both ends induce edge excitations, which lead to an extra $2/N$ in $M/M_{\text{sat}} = 1/5 + 2/N$. The typical $|\phi_i\rangle_{\text{DM}}$ for $L = 8$ is shown in Fig. 8a, b. The RDML state defined in this study does not require $|a_i|^2 = |a_j|^2$ ($i \neq j$). This definition allows for excitation from an RDML state to other RDML states. This is important for understanding the gapless and dispersion-less excitations of $S_{zz}(q, \omega)$. The entanglement spectrum in these dimer–monomer states shows double degeneracy because every state contains a singlet dimer at the center of the chain. The singlet dimer state is represented by $\frac{1}{\sqrt{2}}(|\uparrow\rangle|\downarrow\rangle - |\downarrow\rangle|\uparrow\rangle)$, where the first and second terms have the same absolute value. Therefore, when the singlet dimer is located at the center, the entanglement spectrum must be doubly degenerate. For this reason, we can obtain the double degeneracy even for $L = 2$, where the RDML consists of two dimer–monomer states, $|\phi_{i=1,2}\rangle_{\text{DM}}$ with the central singlet bond, as shown in Fig. 8c, d, respectively.

One may construct RDML states orthogonal to the RDML ground state by changing the distribution of $\{a_i\}$. The constructed RDML state is expected to be in an excited state with infinitesimal or small excitation energy. This corresponds to local excitations, which should form a nearly dispersion-less structure in $S_{zz}(q, \omega)$. The DMRG result shown in Fig. 6 confirms this property. As the size increases, the dispersion-less excitations become more pronounced at approximately $q/\pi = 2$ (see Supplementary Note 3). We note that such a dimensionless spectral distribution depends on the values of $\{a_i\}$ for both the ground and excited states. Similarly, the nonuniformity of the weight of $S_{zz}(q, \omega)$ at approximately $q/\pi = 2$ in Fig. 6a is presumably due to the distribution of $\{a_i\}$. Assuming the presence of the RDML state, we can explain the gapless

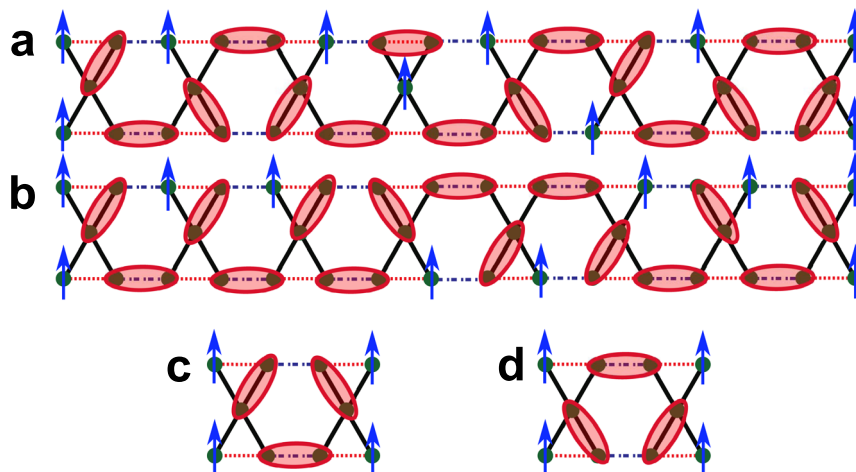


Fig. 8 Schematic diagrams of the dimer–monomer states. Two dimer–monomer states for (a and b) $L = 8$ and (c and d) $L = 2$ under the open boundary condition at $M/M_{\text{sat}} = 1/5 + 2/N$, where L is the number of the 5-site unit, M is the magnetization, and M_{sat} is the saturation magnetization. The green circles denote the sites with spin. The monomers are depicted as blue arrows, whereas the dimers are represented as red ellipses containing two sites. Note that all 5-site units except at both ends in a and b have only one monomer, and there is no nearest-neighboring monomer. The monomers at both ends correspond to the edge excitations.

excitation, double degeneracy of the entanglement spectrum, and dispersion-less low-energy excitations in $S_{zz}(q, \omega)$. Therefore, we believe that phase II is the RDML state.

In summary, we obtained the phase diagram of the 1/5 plateaus of the KSC using the DMRG method. To the best of our knowledge, we discovered two new plateau phases (II and III). As the most surprising result, phase II exhibits a gapless spin liquid with $c=1$ as in the half-integer spin chain and the double degeneracy of the entanglement spectrum as in the spin-1 chain. These features are the same as those of the gapless SPT phases found in previous studies^{38,39}. We also calculated the DSSF in phase II using the DDMRG. We found that the DSSF of $S_{zz}(q, \omega)$ exhibits a gapless excitation corresponding to $c=1$ and dispersion-less low-energy excitations corresponding to local excitations. Finally, we proposed an RDML state that can explain the gapless excitation, double degeneracy of the entanglement spectrum, and dispersion-less low-energy excitations in $S_{zz}(q, \omega)$ in phase II. Based on this proposal, newly derived questions include what symmetry protects the degeneracy during phase II and whether the RDML corresponds to a gapless SPT order.

The KSC compounds with five exchange interactions have been previously reported⁴⁶. Therefore, it is possible that compounds with our model will be synthesized in the future. Because $M/M_{\text{sat}} = 1/5$ is a relatively low magnetization, the 1/5 plateau may be observed experimentally. As such, we anticipate that our study will promote future experimental studies on the KSC.

Methods

We conducted DMRG calculations at zero temperature up to a system size $N = 1000 (= 5 \times 200)$ for various values of J_1 and J_2 . For the system, we construct a snakelike one-dimensional chain. The number of states m kept in the DMRG calculation is 400–2500, and truncation errors are less than 5×10^{-7} . For the calculation of the dynamical spin structure factors, we use DDMRG for $N = 60 (= 5 \times 12)$ and $N = 80 (= 5 \times 16)$ under a periodic boundary condition (PBC). In our DDMRG, we use three kinds of target states: for $S_{zz}(q, \omega)$, (i) $|0\rangle$, (ii) $S_q^z|0\rangle$, and (iii) $(\omega - H + E_0 + i\eta)^{-1} S_q^z|0\rangle$. Target state (iii) is evaluated using a kernel-polynomial expansion method⁴⁰, where the Lorentzian broadening η is replaced by a Gaussian broadening with a width of 0.05. We divide the energy interval $[0, 1.6]$ by 80 mesh points and target all of the points at once with $m = 1000$.

Data availability

The data supporting the findings of this study are available from the corresponding author upon reasonable request.

Code availability

The code that support the findings of this study is not an open source but is available from the corresponding author upon request.

Received: 5 November 2020; Accepted: 22 June 2021;

Published online: 15 July 2021

References

- Horodecki, R., Horodecki, P., Horodecki, M. & Horodecki, K. Quantum entanglement. *Rev. Mod. Phys.* **81**, 865 (2009).
- Blote, H. W. J., Cardy, John, L. & Nightingale, M. P. Conformal invariance, central charge, and universal finite-size amplitudes at criticality. *Phys. Rev. Lett.* **56**, 742 (1986).
- Affleck, I. & Ludwig, A. W. W. Universal noninteger “ground-state degeneracy” in critical quantum systems. *Phys. Rev. Lett.* **67**, 161 (1991).
- Holzhey, C., Larsen, F. & Wilczek, F. Geometric and renormalized entropy in conformal field theory. *Nucl. Phys. B* **424**, 443 (1994).
- Calabrese, P. & Cardy, J. Entanglement entropy and quantum field theory. *J. Stat. Mech.* **2004**, P06002 <https://iopscience.iop.org/article/10.1088/1742-5468/2004/06/P06002> (2004).
- Nishimoto, S. Tomonaga-Luttinger-liquid criticality: numerical entanglement entropy approach. *Phys. Rev. B* **84**, 195108 (2011).
- Pollmann, F., Turner, A. M., Berg, E. & Oshikawa, M. Entanglement spectrum of a topological phase in one dimension. *Phys. Rev. B* **81**, 064439 (2010).
- Zheng, D., Zhang, G.-M., Xiang, T. & Lee, D.-H. Continuous quantum phase transition between two topologically distinct valence bond solid states associated with the same spin value. *Phys. Rev. B* **83**, 014409 (2011).
- Pollmann, F., Berg, E., Turner, A. M. & Oshikawa, M. Symmetry protection of topological phases in one-dimensional quantum spin systems. *Phys. Rev. B* **85**, 075125 (2012).
- Chiara, G., DeLepori, L., Lewenstein, M. & Sanpera, A. Entanglement Spectrum, critical exponents, and order parameters in quantum spin chains. *Phys. Rev. Lett.* **109**, 237208 (2012).
- Haldane, F. D. M. Nonlinear field theory of large-spin Heisenberg antiferromagnets: semiclassically quantized solitons of the one-dimensional easy-axis Neel state. *Phys. Rev. Lett.* **50**, 1153 (1983).
- Anderson, P. W. Resonating valence bonds: a new kind of insulator? *Mater. Res. Bull.* **8**, 153–160 (1973).
- Balents, L. Spin liquids in frustrated magnets. *Nature* **464**, 199–208 (2010).
- Yan, S., Huse, D. A. & White, S. R. Spin-liquid ground state of the $S = 1/2$ Kagome Heisenberg antiferromagnet. *Science* **332**, 1173–1176 (2011).
- Depenbrock, S., McCulloch, I. P. & Schollwock, U. Nature of the spin-liquid ground state of the $S = 1/2$ Heisenberg model on the Kagome lattice. *Phys. Rev. Lett.* **109**, 067201 (2012).
- Nishimoto, S., Shibata, N. & Hotta, C. Controlling frustrated liquids and solids with an applied field in a Kagome Heisenberg antiferromagnet. *Nat. Commun.* **4**, 2287 (2013).
- Mei, J.-W., Chen, J.-Y., He, H. & Wen, X.-G. Gapped spin liquid with Z_2 topological order for the Kagome Heisenberg model. *Phys. Rev. B* **95**, 235107 (2017).
- Ran, Y., Hermele, M., Lee, P. A. & Wen, X. G. Projected-wave-function study of the Spin-1/2 Heisenberg model on the Kagome lattice. *Phys. Rev. Lett.* **98**, 117205 (2007).
- Iqbal, Y., Becca, F. & Poilblanc, D. Valence-bond crystal in the extended Kagome spin-1/2 quantum Heisenberg antiferromagnet: A variational Monte Carlo approach. *Phys. Rev. B* **83**, 100404(R) (2011).
- He, Y.-C., Zaletel, M. P., Oshikawa, M. & Pollmann, F. Signatures of Dirac cones in a DMRG study of the Kagome Heisenberg model. *Phys. Rev. X* **7**, 031020 (2017).
- Liao, H. J. et al. Gapless spin-liquid ground state in the $S = 1/2$ Kagome antiferromagnet. *Phys. Rev. Lett.* **118**, 137202 (2017).
- Marston, J. B. & Zeng, C. Spin-Peierls and spin-liquid phases of Kagome quantum antiferromagnets. *J. Appl. Phys.* **69**, 5962 (1991).
- Syromyatnikov, A. V. & Maleyev, S. V. Hidden long-range order in Kagome Heisenberg antiferromagnets. *Phys. Rev. B* **66**, 132408 (2002).
- Singh, R. R. P. & Huse, D. A. Ground state of the spin-1/2 Kagome-lattice Heisenberg antiferromagnet. *Phys. Rev. B* **76**, 180407(R) (2007).
- Hwang, K., Kim, Y. B., Yu, J. & Park, K. Spin cluster operator theory for the Kagome lattice antiferromagnet. *Phys. Rev. B* **84**, 205133 (2011).
- Ralko, A., Mila, F. & Rousochatzakis, I. Microscopic theory of the nearest-neighbor valence bond sector of the spin-1/2 Kagome antiferromagnet. *Phys. Rev. B* **97**, 104401 (2018).
- Capponi, S., Derzhko, O., Honecker, A., Lauchli, A. M. & Richter, J. Numerical study of magnetization plateaus in the spin-1/2 Kagome Heisenberg antiferromagnet. *Phys. Rev. B* **88**, 144416 (2013).
- Picot, T., Ziegler, M., Orus, R. & Poilblanc, D. Spin-S Kagome quantum antiferromagnets in a field with tensor networks. *Phys. Rev. B* **93**, 060407(R) (2016).
- Schnack, J., Schulenburg, J., Honecker, A. & Richter, J. Magnon crystallization in the Kagome lattice antiferromagnet. *Phys. Rev. Lett.* **125**, 117207 (2020).
- Azaria, P., Hooley, C., Lecheminant, P., Lhuillier, C. & Tsvelik, A. M. Kagome lattice antiferromagnet stripped to its basics. *Phys. Rev. Lett.* **81**, 1694 (1998).
- White, S. R. & Singh, R. R. P. Comment on “Kagome lattice antiferromagnet stripped to its basics”. *Phys. Rev. Lett.* **85**, 3330 (2000).
- Schulenburg, J., Honecker, A., Schnack, J., Richter, J. & Schmidt, H.-J. Macroscopic magnetization jumps due to independent magnons in frustrated quantum spin lattices. *Phys. Rev. Lett.* **88**, 167207 (2002).
- Donkov, A. & Chubukov, A. V. Spin-wave spectra of a Kagome stripe. *Eur. Phys. J. B* **80**, 67005 (2007).
- Shimokawa, T. & Nakano, H. Ferrimagnetism of the Heisenberg models on the quasi-one-dimensional Kagome strip lattices. *J. Phys. Soc. Jpn.* **81**, 084710 (2012).
- Morita, K., Sugimoto, T., Sota, S. & Tohyama, T. Magnetization plateaus in the spin-1/2 antiferromagnetic Heisenberg model on a Kagome-strip chain. *Phys. Rev. B* **97**, 014412 (2018).
- M-Aghaei, A., Bauer, B., Shtengel, K. & Mishmash, R. V. Signatures of gapless fermionic spinons on a strip of the Kagome Heisenberg antiferromagnet. *Phys. Rev. B* **98**, 054430 (2018).
- Acevedo, S., Lamas, C. A., Arlego, M. & Pujol, P. Magnon crystals and magnetic phases in a Kagome-stripe antiferromagnet. *Phys. Rev. B* **100**, 195145 (2019).

38. Scaffidi, T., Parker, D. E. & Vasseur, R. Gapless symmetry-protected topological order. *Phys. Rev. X* **7**, 041048 (2017).
39. Parker, D. E., Scaffidi, T. & Vasseur, R. Topological Luttinger liquids from decorated domain walls. *Phys. Rev. B* **97**, 165114 (2018).
40. Sota, S. & Tohyama, T. Density matrix renormalization group study of optical conductivity in a one-dimensional Mott insulator Sr_2CuO_3 . *Phys. Rev. B* **82**, 195130 (2010).
41. Kennedy, T. Exact diagonalisations of open spin-1 chains. *J. Phys. Condens. Matter* **2**, 5737 (1990).
42. Sato, M. Coexistence of vector chiral order and Tomonaga-Luttinger liquid in the frustrated three-leg spin tube in a magnetic field. *Phys. Rev. B* **75**, 174407 (2007).
43. Plat, X., Capponi, S. & Pujol, P. Combined analytical and numerical approaches to magnetization plateaux in one-dimensional spin-tube antiferromagnets. *Phys. Rev. B* **85**, 174423 (2012).
44. Yonaga, K. & Shibata, N. Ground state phase diagram of twisted three-leg spin tube in magnetic field. *J. Phys. Soc. Jpn.* **84**, 094706 (2015).
45. Oshikawa, M., Yamanaka, M. & Affleck, I. Magnetisation Plateaux in spin chains: “Haldane Gap” for half-integer spins. *Phys. Rev. Lett.* **78**, 1984 (1997).
46. Tang, Y. et al. Synthesis, structure, and magnetic properties of $\text{A}_2\text{Cu}_5(\text{TeO}_3)(\text{SO}_4)_3(\text{OH})_4$ ($\text{A} = \text{Na}, \text{K}$): The first compounds with a 1D kagome strip lattice. *Inorg. Chem.* **55**, 644–648 (2016).

Acknowledgements

We acknowledge discussions with Gonzalo Alvarez from the Center for Nanophase Materials Sciences at ORNL. This study was supported in part by MEXT as a social and scientific priority issue, “Creation of new functional devices and high-performance materials to support next-generation industries (CDMSI),” to be tackled using the post-K computer and MEXT HPCI Strategic Programs for Innovative Research (SPIRE) (hp190198). The numerical calculations were partly conducted at the K Computer and HOKUSAI, RIKEN Advanced Institute for Computational Science, the facilities of the Supercomputer Center, Institute for Solid State Physics, University of Tokyo, and the Information Technology Center, The University of Tokyo. This work was also supported by the Japan Society for the Promotion of Science, KAKENHI (Grant Nos. 19H01829, JP19H05825, and 17K14148), and by JST PRESTO (Grant No. JPMJPR2013).

Author contributions

K.M. conceived the study. K.M. conducted the numerical calculations by DMRG developed by S.S. T.T. conducted the numerical calculations by DDMRG developed by S. S. T.T. supervised the project. All authors contributed to the writing of the manuscript.

Competing interests

The authors declare no competing interests.

Additional information

Supplementary information The online version contains supplementary material available at <https://doi.org/10.1038/s42005-021-00665-6>.

Correspondence and requests for materials should be addressed to K.M.

Peer review information *Communications Physics* thanks the anonymous reviewers for their contribution to the peer review of this work.

Reprints and permission information is available at <http://www.nature.com/reprints>

Publisher's note Springer Nature remains neutral with regard to jurisdictional claims in published maps and institutional affiliations.



Open Access This article is licensed under a Creative Commons Attribution 4.0 International License, which permits use, sharing, adaptation, distribution and reproduction in any medium or format, as long as you give appropriate credit to the original author(s) and the source, provide a link to the Creative Commons license, and indicate if changes were made. The images or other third party material in this article are included in the article's Creative Commons license, unless indicated otherwise in a credit line to the material. If material is not included in the article's Creative Commons license and your intended use is not permitted by statutory regulation or exceeds the permitted use, you will need to obtain permission directly from the copyright holder. To view a copy of this license, visit <http://creativecommons.org/licenses/by/4.0/>.

© The Author(s) 2021